Sternum Age Estimation with Dual Channel Fusion CNN Model

Fuat Türk[1, *], Mustafa Kaya[2], Burak Mert Akhan [2], Sümeyra Çayiröz[2], Erhan Ilgit[2]

[1]Computer Engineering, Cankiri Karatekin University, Cankiri, Turkey
fuatturk@karatekin.edu.tr
[2] Gazi University School of Medicine, Ankara, Turkey

Abstract. Although age determination by radiographs of the hand and wrist before the age of 18 is an area where there is a lot of radiological knowledge and many studies are carried out, studies on age determination for adults are limited. Studies on adult age determination through sternum multidetector computed tomography (MDCT) images using artificial intelligence algorithms are much fewer. The reason for the very few studies on adult age determination is that most of the changes observed in the human skeleton with age are outside the limits of what can be perceived by the human eye. In this context, with the dual-channel Convolutional Neural Network (CNN) we developed, we were able to predict the age groups defined as 20-35, 35-50, 51-65, and over 65 with 73% accuracy over sternum MDCT images. Our study shows that fusion modeling with dual-channel convolutional neural networks and using more than one image from the same patient is more successful. Fusion models will make adult age determination, which is often a problem in forensic medicine, more accurate.

Keywords: Sternum age; deep fusion CNN, CNN age estimation, dual channel fusion CNN, sternum with CNN.

1.   Introduction

Classical age estimation methods usually involve procedures that are detected through images such as the face or finger-wrist bone. The basic principle is to detect the features/findings that occur with aging through images and to estimate age from these features/findings. General machine learning algorithms can be used to estimate age [1]. The accuracy of age estimation over images expressed by machine learning depends on manually designed features and learning algorithms used. A crucial point to note at this point is the fact that a person's biological and skeletal maturity is related to bone age rather than chronological age [2]. Bone age can be used to determine chronological age when information is not available in underdeveloped countries where the age determination of children is not registered [3]. In addition, bone age is used as an auxiliary element in the diagnosis of various diseases [4,5]. Despite the known importance of bone age, studies are mostly limited to the age of 18. The changes

---

* Corresponding author

observed in the skeletal system after the age of 18 are insufficient to make a clear age determination. It is not possible to accurately estimate the digit of a person's chronological age. Age determination in adults can be made with a wide range ranging from ten to twenty years. More precise data is needed in forensic cases where the determination of medical age estimation is extremely important. From this point of view, age determination through the sternum gains importance. However, the fact that there are very few differences in the sternum in individuals who have completed their adulthood, and the inability to make a precise estimation even from the point of view of the radiologist, have caused these studies to be avoided. Therefore, studies have been carried out mostly on height and gender estimation over the sternum [6].

Recently, with the rapid development of Convolutional Neural Networks (CNN), CNNs have been successful in classification problems consisting of close data and have brought the engineering and medical fields together at joint working points. . There are almost no studies on how to construct a highly accurate age estimation model from sternum MDCT images with deep learning methods. With the Dual Channel Fusion CNN (DCF-CNN) model we propose, we carry out the study by transferring coronal and sagittal MDCT images of the sternum to our network via two channels.

The summary of this study and its contribution to science is given below:
1. We offer the opportunity to examine deep learning methods by dividing an original, unused, sternum dataset into groups 20-35, 36-50, 51-65, and over 65 years old.
2. Classic fusion CNN models can have 2,3,4 channels, but they can work by giving the same image as input over and over. Here, we propose a new fusion dual channel model approach by giving coronal and sagittal MDCT images of the same patient as two inputs.
3. Based on the success of the proposed model even in cases where the sternum image differences are very small, we can say that high accuracy values can be achieved by incorporating images with multiple different inputs into the system separately in future studies. This inference is extremely important for difficult deep learning problems.
4. Considering that age estimation studies with the sternum are almost non-existent with deep learning, we should state that we have brought a new perspective with sternum images and directed future studies.
5. We performed the simultaneous extraction and merging of different input images of a system. We demonstrated the use of multiple deep learning models and hyperparameters during this process. As a result, we propose a wide application area by saving deep learning studies from monotonous models.

The study is organized as follows: Sect. 2 summarizes the Literatur survey on the subject. The methodology of the study is given in Sect. 3. The search results are shown in Sect. 4. and Sect. 5 summarizes the conclusion and future works of the study.

2.   Literature Survey

Monum et al. reported that conventional radiographic assessment of ossification of the sternum and rib tips did not yield effective results for age estimation of cadavers. This study examined Computed Tomography (CT) images to determine age at death in the Japanese population. In the study performed on 320 chest plate images, the accuracy of

the model was tested on 26 male and 24 female subjects, and the accuracy in age-decad estimation was found to be 57.69% and 70.83%, respectively [7].

In the study by Singh and Pathak, 8 nonmetric features were examined on 343 sternum images collected from autopsy cases. They observed that the mesosternal foramen is present, especially in men and elderly subjects, and the frequency of lateral projection in the manubrium sterni decreases with aging. It has been suggested that the fusion of sternal elements (manubrium sterni, corpus sterni, and xiphoid process) shows a variable pattern and is therefore not a reliable criterion. Scores of nonmetric features were obtained to the correct gender category in 73.8% and the correct age decades in 70.0% in the logistic regression analysis [8].

Bacci et al. performed an anthropological study on the sternum to estimate the age at death. In this study they mentioned that the sternum is an overlooked element in terms of adult age estimation. Also, fusion phases of 461 sternums from a black South African population were observed to match the individual's actual age with different phases of synostosis of the manubriosternal and sternoxiphoidal connections. The results show that both young (25 years old) and elderly individuals can have the complete fusion of the sternum, while some sternums remain unfused throughout adult life. Overall, logistic regression results showed 62.5% (male = 63.9%; female = 61.8%) accuracy (62.5%) for age determination [9].

Mohammed Ali et al. carried out a study on age and gender estimation in the Egyptian population using MDCT images of the sternum. The validity of the logistic regression equation for gender estimation was calculated as accuracy (88.3%), specificity (90.5%) and sensitivity (85.7%). They stated that the manubriosternal and sternoxiphoidal joint fusions were highly variable according to age, and the general logistic regression results showed a low accuracy rate [10].

Silajiya et al. carried out a study for age estimation on sternum X-Ray images. The authors examined 109 sternum bones and evaluated the fusion of the manubrium sterni and xiphisternum with the sternum body by X-Ray. According to this study, the age of fusion of the xiphisterum and the sternum body in men is 42, and the age of fusion of the xiphisterum and sternum body in women is 44. In the male population, manubriosternal fusion begins at age 50 and is completed after age 59. It has been reported that cases with partial manubriosternal fusion in women increase after the age of 54, and complete union after the age of 64. However, these ages are not exact and belong to a small series studied [11].

Zhang et al. For age estimation based on sternum MDCT images, it examined images of 512 documented individuals (254 females and 258 males) aged 20 to 85 years. In this study, the amount of cartilage costal calcification was taken as a basis for age determination and the Gradient Boosting Regression (GBR), Support Vector Machine (SVM) and Decision Tree Regression (DTR) machine learning models were tested. Outcomes were estimated at 88% for men and 77% for women [12].

When the literature is evaluated as a whole, it is seen that the studies that are more successful in age estimation are those based on the amount of calcification in the cartilaginous component of the ribs. Studies based on the fusion of the manubrium sterni and processus xiphoideus with the corpus sterni were able to estimate age with less accuracy.

3.   Methodology

3.1.   Dataset and Image Preprocessing

The data set used in this study was meticulously prepared by Radiologist Doctor Mustafa Kaya and his team, with the approval of the ethics committee of Gazi University. MDCT images of the study were obtained from patients who underwent thoracic MDCT for any reason between 01/01/2021 and 30/06/2022 in the Department of Radiology, Faculty of Medicine, Gazi University. MDCT examinations were performed with a third generation 192 section, dual tube MDCT scanner (Somatom Force, Siemens Healthcare, Erlangen, Germany) using the following parameters. Tube output 120 kV, pitch 0.9, detector collimation 0.6 mm, reconstruction section thickness 1 mm. The HU value of the sternum medullary, the width of the joint space between the corpus sterni and the manubrium sterni, and the amount of calcification of the anterior cartiloginous components of the ribs 1-7 were evaluated. Patients over 20 years of age who had not undergone mediastinotomy were included in the study. Investigations with movement/respiratory artifacts, artifacts caused by metallic stabilization bodies belonging to previous operations, and artifacts of port or cardiac pacemakers were excluded from the evaluation. In the study, MDCT images of a total of 300 patients, 75 in each class, including four different age groups, 20-35, 36-50, 51-65, and over 65, were used. Information about data distribution is shown in Figure1.
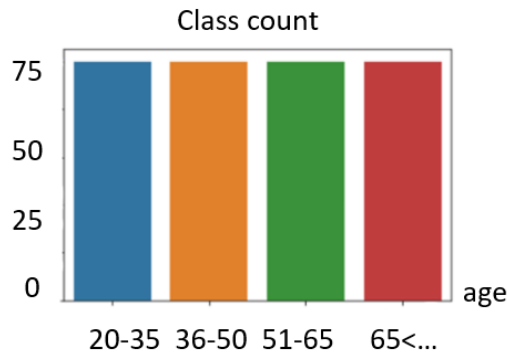
Fig. 1. Sternum dataset distribution graph.

The hypotheses for age determination are given in the following three titles.
1. As the age increases, the joint distance between the corpus sterni and the manubrium sterni narrows.
2. As the age increases, the medullary Hounsfield Unit (HU) density of the sternum decreases.
3. As the age increases, the amount of calcification of the cartilage costae, which forms the costosternal joints, increases.
   To evaluate these hypotheses, the following measurements were made.
1. The joint distance between the corpus sterni and the manubrium sterni was measured from the 2D sagittal sternum MDCT image.

2. To rule out the effect of possible degenerative effects on the manubriosternal joint, medullary HU values were measured with a 5 mm diameter ROI (Region of interest) from the manubrium stern approximately 1 cm superior to the manubriosternal joint and from the corpus stern approximately 1 cm superior to the xiphoid process proximal line.

3. Multipanar reconstruction (MPR) was performed in the coronal plane, and Maximum Intensity Projection (MIP) images of 15 mm thickness were obtained from the coronal section including the second costosternal joint. It was aimed to evaluate the amount of calcification in the cartilage component of the bilateral ribs 1-7 on the defined MIP images. The measurements are explained in detail in Tables 1, 2, and 3.

Table 1. Values of manubriosternal joint space by age groups

| Age range	Manubriosternal-joint spacing median value (mm)	Manubriosternal-joint spacing mean ± SD (mm)
20-35	2.4	2.1 ± 1.3
36-50	2.1	2.0 ± 1.1
51-65	2.0	2.0 ± 1.3
65<...	1.5	1.5 ± 1.3

Table 2. Manubrium sterni HU values

Age range	ManubriumHU (mean±SD)	ManubriumHU(median)	ManubriumHU percentile< %5	ManubriumHU percentile>%95
20-35	214 ± 75	218	73	333
36-50	161 ± 58	169	29	243
51-65	129 ± 66	129	5	239
65<...	99 ± 74	108	-27	227

Table 3. Korpus sterni HU values

| Age range	KorpusHU (mean ±SD)	KorpusHU (median)	KorpusHU percentile <%5	ManubriumHU percentile >%95
20-35	128 ± 69	124	29	244
36-50	76 ± 57	82	-18	175
51-65	59 ± 69	54	-46	174
65<...	27 ± 62	33	-27	124

Existing images were edited with the help of the Pillow library within the Python Imaging Library by making Crop, Contrast, Brightness, and Filter improvements, respectively. Due to the high similarity between patient classes, additional image processing, and data augmentation techniques were not particularly preferred. The data obtained from the image processing results are shown in Figure 2.
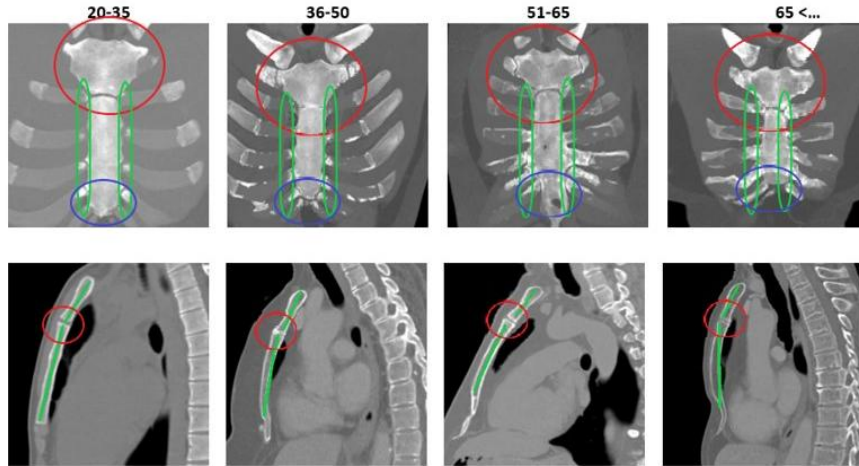
Fig. 2. Sternal age group images after image processing. Top row: Red ring: Configuration changes in the manubrium stern with age, green ellipse: Increasing calcification of the costosternal joints with age, Blue ring: Configuration changes observed in the xiphoid process. Bottom row: Manubriosternal narrowing and increase in subchondral sclerosis with age.

3.2.   Classic CNN Classification

Classification with CNN is the most widely used architecture in difficult classification problems such as histopathological typing of tumors, in the differentiation of benign or malignant masses on radiological images [13-15]. Medical Imaging studies often attract attention as studies with limited data. To overcome the difficulties in such studies, a pre-trained network with a different dataset can be used by adapting it to the classification task. These networks, developed , produce promising results in various medical imaging studies but the results are always open to discussion. In this case, the best way to follow would be to design CNN models that can recognize the network model well even under difficult classification conditions. Figure 3 shows a basic CNN architecture.
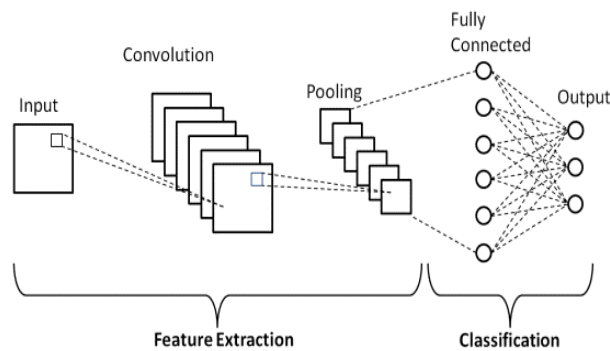
Fig. 3. Basic CNN architecture

The basic network structure starts with the image, where the image is filtered to include maps in the convolution layer. It is then condensed with pool layers. Subsequently, higher-level features are extracted in fully connected layers with a corresponding weight. These achievable features are processed to classify according to output categories corresponding to the original input. [16,17].

3.3.   Proposed DCF-CNN architecture

With Fusion CNN architectures, it is aimed to learn architecture better by giving the same scene as an input again and again. The ultimate goal here can also be considered as capturing more features with fewer modalities [18,19].

Coding the basic information for the architectural structure allows a learning level without a large amount of data, so the use of a small-scale dataset provides successful results in terms of performance [20].

The fusion model design shown in the figure below is inspired by the Hybrid V-Net model and fusion deep neural network architectures [21]. The proposed Fusion based CNN architecture is shown in Figure 4.
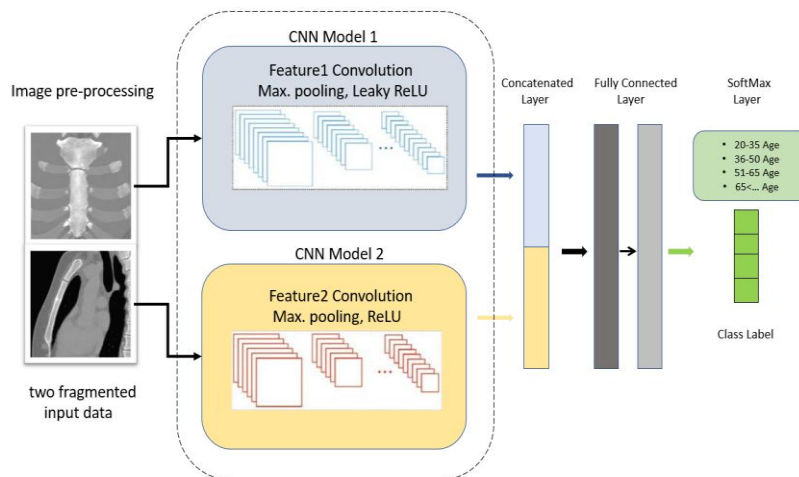

Fig. 4. Proposed DCF-CNN architecture

This work presents a DCF-CNN architecture to generate many local structures with various filter sizes. The input image size for the proposed DCF-CNN architecture is $150 \times 150 \times 3$. The main entrance is divided into two roads. These include the CNN Model1 and CNN Model2 architectures. Login information is given parallel to these paths. The proposed architectures include convolutional filter size layers of 5×5 and 3×3, respectively. More local features are obtained with these filters of different sizes. In both Model paths, maximum pooling and Batch Normalization (BN) operations are performed after the convolution operations. One of the obvious differences between the models was the preferred activation functions. Leaky ReLU activation was used as it gave better results for CNN Model1. Thus, we can say that we can achieve more

optimization of the network by eliminating the negativities arising from large gradients. The Leaky ReLU activation Function is shown in Equation 1. Although the coefficient "a" expressed here is a small value, it was preferred as 0.01 for our model [22].

$$f(x) = \begin{cases} x & if\ x > 0, \\ ax & otherwise \end{cases} \qquad (1)$$

For CNN Model2, the ReLU activation function is preferred and is shown in Equation 2. It should be noted that values less than zero are neglected and it is aimed to optimize accordingly [23].

$$f(x) = \max(0, x) \qquad (2)$$

Another difference between the two architectures is the optimization method. Just as Adam is essentially an RMSprop with momentum, so Nadam is Adam with Nesterov momentum. Adam is an extension of gradient descent that adds the first and second moments of the gradient and automatically adapts a learning rate for each optimized parameter. Nadam, on the other hand, is a momentum extension where the update is performed using the gradient of the predicted update in the parameter instead of the actual current variable value. This has the effect of slowing down the search when optimizing is found rather than overdone in some cases [24,25]. For this reason, Adam for the first model and the Nadam optimizer for the second model was preferred because they gave better results. To better understand the implementation phase of the proposed models, the layer structures, activation functions, and dropout blocks are shown in Table 4. It should be noted here that two different architectural features were combined during classification after the extraction stage and turned into a fully connected single-layer structure. This structure allows the same input class to capture more features with more than one image, rather than combining two images with a single image.

Table 4. CNN Model1 and CNN Model2 structures

	CNN Model 1	CNN Model2
Input Image	150*150*3	150*150*3
Filters size	256/128/64/32/16	256/128/64/32/16
Kernel size	(5,5)/(5,5)/(3,3)/(3,3)/(3,3)	(5,5)/(5,5)/(3,3)/(3,3)/(3,3)
Pool. Layer	Max. Pool (2,2)	Max. Pool (2,2)
Optimizer	Adam Optimizer	Nadam Optimizer
Activation	Leaky ReLU	ReLU
Concat. Layer	256*2	
Fully Con.	512/256/4	
Output	Softmax, 4 class	

3.4.   Performance Evaluation Metrics

Accuracy, Recall, Precision, and F-measure are the main metrics for measuring the performance of classification algorithms. Accuracy describes the overall performance of the proposed model and is calculated as shown in Equation 3 [26].

$$Accuracy = \frac{TP+TN}{TP+TN+FP+FN} \qquad (3)$$

Precision shows how many of the Positive predicted values are Positive and is calculated as shown in Equation 4.

$$Precision = \frac{TP}{TP+FP} \qquad \textbf{(4)}$$

A recall is a measure of how many transactions that should have been predicted as Positive were predicted as Positive and is calculated as shown in Equation 5.

$$Recall = \frac{TP}{TP+FN} \qquad \textbf{(5)}$$

The F1-Score value shows the harmonic mean of the Precision and Recall values and is calculated as shown in Equation 6.

$$F1 - score = \frac{2*Precision*Recall}{Precision+Recall} \qquad \textbf{(6)}$$

3.5.   Dataset Distribution Operations

Figure 5 shows the block diagram of how the distribution is made. The point to note here is that two different images of patients with the same Identification Number (ID) are given sequentially as input to the two proposed models. To ensure the distribution, the ID information of the data set given to the first model was transferred to the second model.
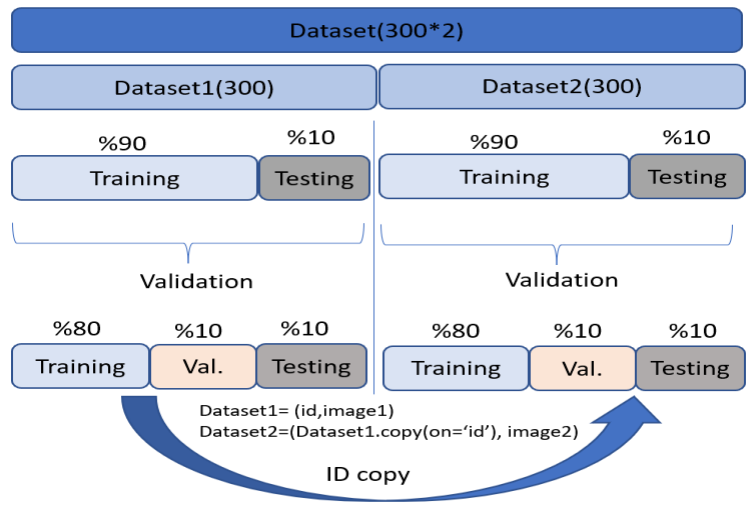

Fig. 5. Dataset Separation Process

4.   Results and Discussion

The results shown in this section show the data obtained as a result of the train, test, and validation stages and the distribution of the data set. Fusion Model and CNN Models were run separately with 100 epochs. Each model is trained as designed with the same

hyperparameters. In Figure 6, accuracy and loss curves for the proposed Fusion CNN model after training and test results are shown. Based on these curves, we can easily say that the training and test results are consistent. However, the learning process could not go higher after a point.
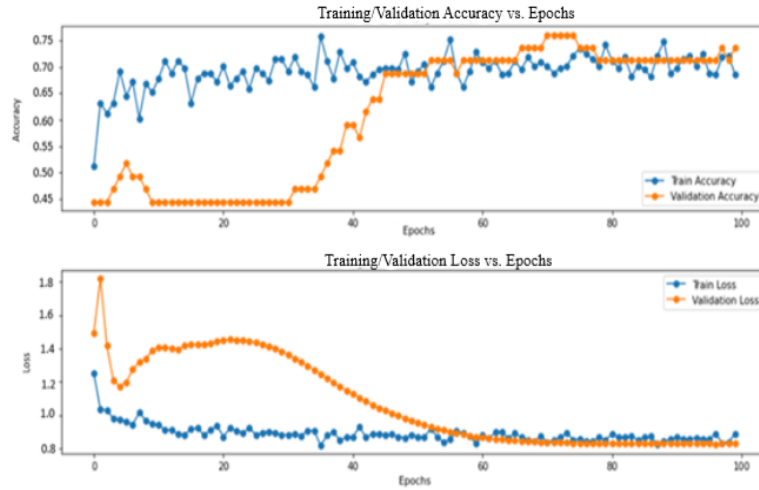
Fig. 6. Train and validation accuracy/loss graph for DCF-CNN

Table 5 shows the performance metrics after the test results of the values with all three models together. When the results were examined, CNN Model1 was run only on coronal images for the sternum and achieved 65% accuracy, while CNN Model2 only achieved 61% accuracy on sagittal images. The dual-channel Fusion CNN Model we recommend, on the other hand, took coronal and sagittal images together as input and achieved an accuracy rate of 73%.

Table 5. CNN models and proposed DCF-CNN of metrics values

Model	Accuracy	Precision	Recall	F1-Score
CNN Model1	0.65	0,66	0.67	0.66
CNN Model2	0.61	0.62	0.62	0,61
DCF-CNN Model	0.73	0.73	0.74	0.74

When the confusion matrix table in Figure 7 is examined, we can say that there are deviations in the results of the estimation values, especially due to the close differences between the ages of 36-50 and 51-65. However, the high similarities between the image classes and the existence of exceptional cases that can be observed in all age groups make age estimation very difficult for radiologists.
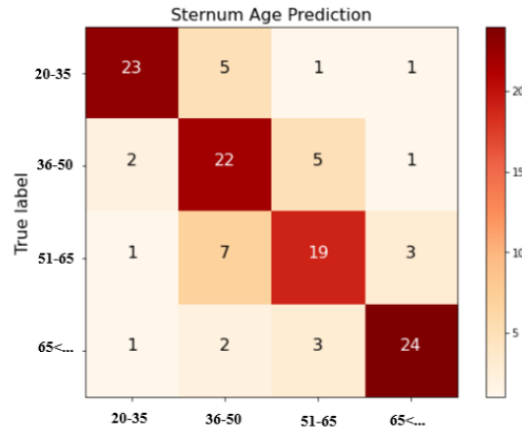
Fig. 7. Sternum age confusion matrix graph for DCF-CNN

In Figure 8, examples where the models are mislabeled for both images are given. Based on these images, it is seen that there are false labels not only in close classes but also in classes with high age differences. Looking at the images, it can be seen how difficult the classification task is. It is understood that only very small differences are decisive. We thought that the decrease in sternum medullary HU values with age might be a correction factor in the estimated age and actual age mismatches, but our results did not support this. Measured sternum meduller HU values were consistent with the estimated age, not the actual age. This made us think that the osteoporotic process in the sternum that develops with age is not a parameter independent of changes in the shape of the sternum bone or calcifications in the cartilage costa. The osteoporotic process is almost always related to bone shape changes with age, and probably the main cause of bone shape changes is the osteoporotic process. In addition, meduller HU measurements on the sternum for age groups are valuable and HU values below 5% percentile can be used as reference values for the diagnosis of osteoporosis.
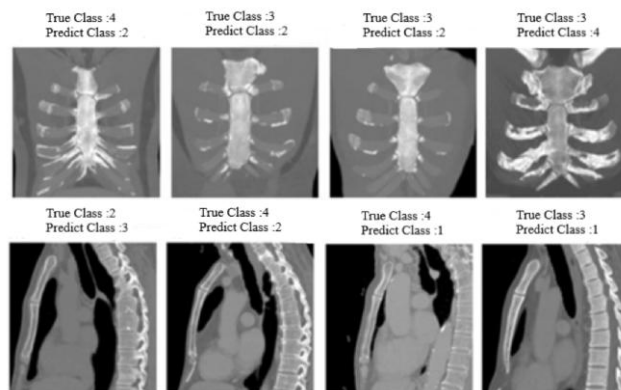

Fig. 8. Sternum mislabel images, Class 1: 20-35 age, Class 2: 36-50 age, Class 3: 51-65 age, Class 4 : 65<… (DCF-CNN test result)

The most successful study for age determination on sternum MDCT images is the study published by Zhang et al. in 2018 [12]. Although manubriosternal joint space and sternum medullary HU values were also included in the evaluation for a more precise age determination in our study, we could not determine age with precision in this study. The reason for this may be that individuals with chronic diseases that will affect age determination were not excluded from our dataset. In addition, while Zhang et al used the images obtained with the volume rendering technique (VRT) for age determination, we preferred 2D MIP images. With a high probability, VRT images are more successful in age determination than 2D MIP images.

5.   Conclusions

Sternum age estimation studies carried out to date include classical biostatistics studies based on logistic regression analyzes based on the human eye, or machine learning studies that do not suggest a new model. With the DCF-CNN model we proposed, we were able to predict with 73% accuracy the original data set, which we divided into four diverse groups (with a 15-year interval) on a challenging subject with natural limitations such as adult age determination. The fusion modeling, we developed on two separate images of the sternum in our study increased our success compared to the predictions made with a single image. Based on this situation, we present a new approach model that will make a difference, especially in medical images. We can state that the success of the system can be increased by using images of the same patient with unique features related to each other. Even other than the medical image, two or more images with the same features can be passed through multiple channels and the accuracy can be increased by combining common features. In this context, we can say that more efficient results can be obtained by using different optimization methods, activation functions and hyperparameters at the same time.

As a future perspective, more advanced fusion models can be used on other bones used in adult age determination, especially pelvis bones, and studies are needed in this direction.

References

1. Xing, J., Li, K., Hu, W., et al. Diagnosing deep learning models for high accuracy age estimation from a single image. Pattern Recognition, Vol 66, 106–116. (2017) https://doi.org/10.1016/J.PATCOG.2017.01.005
2. Mirwald, RL., Dominic, A., Baxter-Jones G., Bailey DA. An assessment of maturity from anthropometric measurements Pediatric Bone Mineral Accrual Study View project Growth and Maturation in Sport and Exercise View project (2002) https://doi.org/10.1097/00005768-200204000-00020
3. Setel, P.W., Macfarlane, S.B., Szreter, S, et al. Who Counts? 1 A scandal of invisibility: making everyone count by counting everyone. Vol 370, 1569–77, (2007). https://doi.org/10.1016/S0140
4. Satoh, M. Bone age: assessment methods and clinical applications. Clinical Pediatric Endocrinology, Vol 24, 143–152, (2015). https://doi.org/10.1297/CPE.24.143

5. Nguyen, Q.H, Nguyen, B.P, Nguyen, M.T., et al. Bone age assessment and sex determination using transfer learning. Expert Systems with Applications, Vol 200, 116926, (2022). https://doi.org/10.1016/J.ESWA.2022.116926

6. Saraf, A., Kanchan, T., Krishan, K., et al. Estimation of stature from sternum-Exploring the quadratic models, (2018). https://doi.org/10.1016/j.jflm.2018.04.004

7. Monum, T., Makino, Y, Prasitwattanaseree ,S, et al. Age estimation from ossification of the sternum and true ribs using 3D post-mortem CT images in a Japanese population, (2019). https://doi.org/10.1016/j.legalmed.2019.101663

8. Singh,J., Pathak, RK. Forensic Anthropology Population Data Sex and age-related non-metric variation of the human sternum in a Northwest Indian postmortem sample: A pilot study, (2013). https://doi.org/10.1016/j.forsciint.2013.02.002

9. Bacci, N, Nchabeleng, EK., Billings, BK Forensic Anthropology Population Data Forensic age-at-death estimation from the sternum in a black South African population, (2017). https://doi.org/10.1016/j.forsciint.2017.11.002

10. Ismail, M., Ali, M., Mosallam, W., et al Sternum as an indicator for sex and age estimation using multidetector computed tomography in an Egyptian population. Forensic Imaging Vol, 26, 200457, (2021). https://doi.org/10.1016/j.fri.2021.200457

11. Radiological Age Estimation From Sternum.: EBSCOhost. Available: https://web.p.ebscohost.com/ehost/pdfviewer/pdfviewer?vid=0&sid=0b6e5d68-86f6-44f4-aaa6-9b3a8c6e9271%40redis, (2022).

12. Zhang, K, Fan, F, Tu, M, et al. The role of multislice computed tomography of the costal cartilage in adult age estimation. International Journal of Legal Medicine, Vol 132, 791–798, (2018). https://doi.org/10.1007/S00414-017-1646-Y/TABLES/3

13. Abdullahi, A., Bawazeer, K., Alotaibai, S, et al. Pretrained Convolutional Neural Networks for Cancer Genome Classification; Pretrained Convolutional Neural Networks for Cancer Genome Classification, (2020).

14. Sun, Y., Zhu, S., Ma, K., et al. Identification of 12 cancer types through genome deep learning. Scientific Reports 2019, Vol 9, No. 1, 1–9, (2019). https://doi.org/10.1038/s41598-019-53989-3

15. Li, S., Xu, P., Li, B, et al Predicting lung nodule malignancies by combining deep convolutional neural network and handcrafted features. Physics in Medicine & Biology Vol. 64, 175012, (2019).. https://doi.org/10.1088/1361-6560/AB326A

16. Ardila, D., Kiraly, AP., Bharadwaj S, et al. End-to-end lung cancer screening with three-dimensional deep learning on low-dose chest computed tomography, (2019). https://doi.org/10.1038/s41591-019-0447-x

17. Mutasa, S., Sun, S, Ha, R. Understanding artificial intelligence-based radiology studies: CNN architecture. Clinical Imaging, Vol, 80, 72–76, (2021). https://doi.org/10.1016/J.CLINIMAG.2021.06.033

18. Türk, F., Lüy, M., Barışçı, N. Kidney and Renal Tumor Segmentation Using a Hybrid V-Net-Based Model. Mathematics 2020, Vol 8, 1772 (2020). https://doi.org/10.3390/MATH8101772

19. Zhang, Y., Morel, O., Blanchon, M., et al. Exploration of Deep Learning-based Multimodal Fusion for Semantic Road Scene Segmentation. VISIGRAPP 2019 - Proceedings of the 14th International Joint Conference on Computer Vision, Imaging and Computer Graphics Theory and Applications, Vol 5, 336–343, (2019). https://doi.org/10.5220/0007360403360343

20. Mezina, I., Qingjie, L., Yunhong, W. Very High-Resolution Images Classification by Fusing Deep Convolutional Neural Networks, The 5th International Conference on Advanced Computer Science Applications and Technologies ,(2017). https://doi.org/10.23977/ACSAT.2017.1022

21. Tenenbaum, J.B, Freeman, W.T. Separating style and content with bilinear models. Neural Computation, Vol, 12, 1247–1283, (2000). https://doi.org/10.1162/089976600300015349

22. Maniatopoulos, A., Mitianoudis, N. Learnable Leaky ReLU (LeLeLU): An Alternative Accuracy-Optimized Activation Function, (2021). https://doi.org/10.3390/info12120513

23. Eckle, K., Schmidt-Hieber, J. A comparison of deep networks with ReLU activation function and linear spline-type methods. Neural Networks, Vol 110, 232–242, (2019). https://doi.org/10.1016/J.NEUNET.2018.11.005
24. Khaire, U.M., Dhanalakshmi, R. High-dimensional microarray dataset classification using an improved adam optimizer (Adam). Journal of Ambient Intelligence and Humanized Computing, Vol 11, 5187–5204, (2020). https://doi.org/10.1007/s12652-020-01832-3
25. Sharma, J., Soni, S., Paliwal, P., et al. A novel long-term solar photovoltaic power forecasting approach using LSTM with Nadam optimizer: A case study of India, (2022). https://doi.org/10.1002/ese3.1178
26. Nisha, J.P., Gopi, V., Palanisamy, P. Automated colorectal polyp detection based on image enhancement and dual-path CNN architecture. Biomedical Signal Processing and Control Vol, 73, 103465, (2022). https://doi.org/10.1016/J.BSPC.2021.103465

Fuat Türk B.Sc. graduated from Gazi University Computer Technology Department in 2004. He received his PhD degree from K ırı kkale University Computer Engineering Department in 2020. He is working as an Assistant Professor in the Department of Computer Engineering at Çankırı Karatekin Univers ity. His areas of interest are biomedical informatics, artificial intelligence and software.

Mustafa Kaya, MD. graduated from Ankara University Medical School in 1996. He finished radiology residency at the Ankara University Medical School in 2002. He is working as Lecturer in the Department of Radiology at Gazi University Medical School. He is an expert in thoracic and abdominal Multi detector CT imaging.

Burak Mert Akhan, MD. graduated from Hacettepe University, Faculty of Medicine in 2017. She is working as a Resident Doctor in the Department of Radiology at Gazi University Faculty of Medicine since 2019. His areas of interest are interventional radiology and artificial intelligence.

Sumeyra Çayıröz, MD. graduated from Istanbul University, Istanbul Faculty of Medicine in 2020. She is working as a Resident Doctor in the Depa rtment of Radiology at Gazi University Faculty of Medicine since 2021.

Erhan Ilgıt MD. graduated from Ankara University Medical School in 1986. He finished Radiology residency at the Gazi University Medical School in 1991. He became associate professor in 1993 and full professor in 2011. He serves as the Director of the Radiology D epartment at Gazi University Medical School.